Published in final edited form as:
Nat Cell Biol. 2011 April ; 13(4): 361–370. doi:10.1038/ncb2206.

Drosophila Katanin is a microtubule depolymerase that regulates cortical-microtubule plus-end interactions and cell migration

Dong Zhang[1], **Kyle D. Grode**[2,#], **Shannon Stewman**[1,#], **Daniel Diaz**[3,#], **Emily Liebling**[1], **Uttama Rath**[1], **Tania Riera**[1], **Joshua Currie**[2], **Daniel W. Buster**[4], **Ana B. Asenjo**[1], **Hernando J. Sosa**[1], **Jennifer Ross**[3,#], **Ao Ma**[1,#], **Stephen L. Rogers**[2,#], and **David J. Sharp**[1,*]

[1]Department of Physiology and Biophysics, Albert Einstein College of Medicine, 1300 Morris Park Avenue, Bronx, NY 10461

[2]Department of Biology and the Center for Carolina Genome Sciences, University of North Carolina, Chapel Hill, 421 Fordham Hall, CB# 3280, Chapel Hill, NC 27599

[3]Department of Physics, University or Massachusetts, Amherst, 302 Hasbrouck Laboratory, Amherst, MA 01003

[4]Department of Cell Biology and Anatomy and the Arizona Cancer Center, University of Arizona, Tuscon, 1515 N. Campbell Avenue, Tuscon, AZ 85724

Abstract

Regulation of microtubule dynamics at the cell cortex is important for cell motility, morphogenesis and division. Here we show that the *Drosophila* Katanin, Dm-Kat60, functions to generate a dynamic cortical-microtubule interface in interphase cells. In S2 cells, Dm-Kat60 concentrates at the interphase cell cortex where it suppresses the polymerization of microtubule plus-ends thereby preventing the formation of aberrantly dense cortical arrays. Dm-Kat60 also localizes to the leading edge migratory D17 cells and negatively regulates multiple parameters of their motility. Finally, *in vitro*, Dm-Kat60 severs and depolymerizes MTs from their ends. Based on these data, we propose that Dm-Kat60 removes tubulin from microtubule ends or lattice that contact specific cortical sites to preventing stable and/or lateral attachments. The asymmetric distribution of such an activity could help generate regional variations in MT behaviors involved in cell migration.

Introduction

Microtubules (MTs) form complex and dynamic arrays with pivotal roles in the development and function of eukaryotic cells. While MTs are intrinsically dynamic, their cellular behaviors are tightly regulated by a host of additional factors[1,2]. Thus, the MT

*Correspondence should be addressed to David J. Sharp, david.sharp@eintsein.yu.edu.
#These authors contributed equally

Author contributions: DZ carried out and analyzed most experiments using Drosophila S2 and human cells. DZ also purified and performed the initial *in vitro* characterization of rDm-Kat60. KDG performed the majority of experiments with Drosophila D17 under the direction of SLR. JC also performed analyses in D17 cells. SS designed the automated tracking algorithm under the direction of AA and used it to track MTs in live cell movies provided by DZ. DD and JR performed numerous in vitro assays to quantify the MT severing and end-depolymerase activities of rDM-Kat-60. ABA, EL and TR performed and analyzed the EM under the direction of HJS. UR performed KLP59D for the EM assay. DWB helped in the design of many experiments in S2 cells and made the model figure shown in supplementary information. DJS wrote the manuscript (with the help of all authors but particularly SLR) and coordinated the efforts of the multiple labs involved in this project.

cytoskeleton is responsive to a variety of cues and can locally adapt its dynamic properties accordingly. These regulatory inputs appear to be particularly relevant at the cell cortex where localized alterations in MT dynamics and organization are central to cell migration, polarization, morphogenesis, and division[3–6].

Katanin is a phylogenetically conserved enzyme which utilizes the energy of ATP hydrolysis to generate MT breakage, *in vitro*[7]. Katanin was originally purified from sea urchin eggs as a heterodimer of a 60 kD catalytic subunit (p60) and an 80 kD targeting and regulatory subunit (p80)[8]. Katanin p60 and p80 homologues have now been identified in evolutionary diverse systems and many organisms contain several genes encoding distinct p60 and/or p80 proteins. Functional analyses reveal diverse roles for Katanin in mitosis/meiosis[9–12], neuronal morphogenesis[13,14], and the assembly/disassembly of cilia/flagella[15–18]. In addition, a Katanin in higher plants has been shown to regulate the assembly of cortical MT arrays which, in turn, determine the directional deposition of cellulose and thus impact cell morphogenesis[19–22]. In this context, Katanin releases new MTs nucleated from the walls of pre-existing MTs[7,23].

We previously found that the *Drosophila* Katanin p60, Dm-Kat60, associates with mitotic chromosomes and stimulates the depolymerization of kinetochore-associated MT plus-ends during anaphase A[12]. In the present study, we tested the hypothesis that Dm-Kat60 also functions to regulate MT dynamics during interphase - a topic that has not been addressed in any other animal system.

Results

Dm-Kat60 localizes to the interphase cell cortex

We first probed Dm-Kat60's localization in cultured interphase S2 cells using immunofluorescence. Dm-Kat60 immunostaining was found to be strongly enriched within a 0.5–3 μm thick band extending around the entire cell boundary (Fig. 1a). This cortical staining pattern was reduced or abolished by Dm-Kat60 RNAi supporting its specificity (see Supplementary information, Fig. S1a). Ectopically-expressed Dm-Kat60-GFP also acquired a cortical localization (see Supplmentary information, Fig. S2 a,b).

Though Dm-Kat60 showed little co-localization with MTs in the interphase cell interior, numerous MT plus-ends were observed to extend into and terminate within the Dm-Kat60-rich cortical zone (Fig. 1b,c). Dm-Kat60 also generally co-localized with cortical actin (Fig. 1d). Dm-Kat60's cortical localization occurs independently of MTs as it persists following MT depolymerization with colchicine. However, it is nearly completely abolished when cells are treated with cytochalasin D indicating a strong reliance on actin (see Supplementary information, Fig. S3). On the other hand, Dm-Kat60 RNAi did not prevent the cortical accumulation of actin (see Supplementary information, Fig. S1b).

Dm-Kat60 regulates interphase MTs

We then performed live analyses of MT behaviors in control and Dm-Kat60 RNAi-treated S2 cells expressing GFP-α-tubulin. In controls, MTs generally grew perpendicularly to the cortex, briefly paused upon contacting the cortex, and then catastrophed (transition from growth to shrinkage) into the cell interior (Fig. 2a; Movie S1a; see also [24]). >90% of plus-end catastrophes (78/84 observed in 9 cells) occurred within 3 μm of the cell edge indicating the Dm-Kat60-rich cortical zone as a potential "hot-spot" for the induction of MT depolymerization.

Interestingly, some MTs were also observed to break very near their ends upon contacting the cortex. The newly formed plus-ends of these "severed" MTs initiated catastrophe

immediately thereafter (Fig. 2b; Movie S1c). While such events were rarely observed when cells were imaged at 5 second intervals (our standard for longer time-series), they appeared much more frequently when images were acquired at subsecond intervals (0.2–0.8 images/second). Under these conditions, putative severing events near MT tips preceded ~30% of observed catastrophes (20/63 microtubule catastrophes observed in 7 cells).

In stark contrast to controls, MTs in the majority of Dm-Kat60-depleted cells were noticeably curled beneath the cortex and often formed dense parallel arrays ringing the cell periphery (Fig. 2c; Movie S1b). This phenotype was largely reversed by the induced expression of an RNAi-resistant Dm-Kat60-GFP construct (see Supplementary information, Fig. S2c,d). While we were unable to observe the formation of these cortical arrays *de novo*, examination of the few clearly visible individual MTs present at the onset of imaging provided insights into their genesis. Similarly to controls, these MTs often contacted the cortex plus-end on. However, instead of rapidly initiating catastrophe, they continued to grow along the cortex until coming into proximity of the underlying ring of MTs, into which they were ultimately incorporated (Fig. 2d).

A unique role for Dm-Kat60 in MT dynamic instability

Roughly a quarter of the Dm-Kat60 RNAi-treated interphase S2 cells imaged contained at least some cortical domains with numerous unambiguously identifiable MT plus-ends. The behaviors of these were analyzed in detail. To measure large numbers of plus-end behaviors, we developed an automated tracking algorithm which could accurately follow the position of MT ends over time (Fig. 3a; Movie S1d,e; see Methods). The validity of this approach was confirmed by comparing a subset of MT trajectories generated automatically to those generated by hand (see Supplementary information, Fig. S3).

Consistent with our visual inspection of the data, in controls, the majority of MT plus-end growth/shrinkage trajectories occurred along largely straight paths oriented perpendicular to the cortex (Fig. 3b). By contrast, Dm-Kat60 RNAi cells displayed numerous plus-end trajectory paths parallel to the cortex (Fig 3c). Moreover, on average, MT plus-ends in Dm-Kat60 RNAi cells spent significantly more time in growth (as opposed to shrinkage) parallel to the cortex and were positioned significantly closer to the cell edge (Fig. 3d,e).

We then analyzed the life history plots of the tracked plus-ends to specify Dm-Kat60's impact on dynamic instability (Table 1). As expected, Dm-Kat60 RNAi significantly suppressed plus-end catastrophes >2-fold. Thus, Dm-Kat60 is normally a potent catastrophe promoter. Dm-Kat60 depletion also increased transitions from pause to growth; paused plus-ends were almost twice as likely to rescue to the growth state. Surprisingly, the frequency of the reverse transition (a growing plus-end stalling into pause) also increased after Dm-Kat60 RNAi, but by a more modest 20%. Finally, we measured a slight (~20%) but significant increase in MT growth rate in Dm-Kat60 RNAi cells. On the other hand, depletion of Dm-Kat60 did not significantly impact the frequency of transitions out of the shortening state nor did it alter the average rate of shrinkage.

The *Drosophila* Kinesin-13, KLP10A, has also been found to promote catastrophes at cortex of interphase S2 cells[24]. To better understand Dm-Kat60's functional inter-relationship with this protein, we reassessed KLP10A's influence on MT dynamics using our current methodologies (Table 1). As with Dm-Kat60 RNAi, the depletion of KLP10Asignificantly reduced catastrophe frequency. However, KLP10A RNAi also increased the frequency of transitions into pause--Kat60 RNAi had the opposite effect. Also unlike Dm-Kat60 RNAi, KLP10A RNAi had no influence on MT growth rate but strongly suppressed the rate of shrinkage.

Dm-Kat60 localizes to the leading edge of D17 cells and regulates their migration

Dm-Kat60's influence on MT dynamics at the cell cortex suggested a role in cell migration[25–28]. Since S2 cells are immotile, we examined this possibility in migratory D17 cells. D17 cells were originally isolated from cultures of dissected imaginal discs[29]; despite their epithelial origin, D17 cells exhibit a gene expression profile that is consistent with that of *Drosophila* hemocytes (data not shown). Like hemocytes[30–32], D17 cells spontaneously polarize in culture, assemble an exaggerated leading edge, and exhibit robust cell motility (Movie S2). Immunofluorescence revealed that Dm-Kat60 accumulates at the leading edge of polarized D17 cells where it extensively co-localizes with actin (Fig. 4a). The other MT-severing enzymes in *Drosophila*, Spastin and Fidgetin[12,33], displayed no such cortical enrichment nor did their depletion obviously alter D17 cell migration (see Supplementary information, Fig. S5).

Dm-Kat60's influence on D17 cell migration was first examined in a wound healing assay. D17 cell cultures were treated with Dm-Kat60 or control dsRNA for 10 days, the confluent monolayers were wounded with a pipette tip, and the resulting "wounds" were imaged immediately and 24 h later. Unexpectedly, we measured a significant 1.4-fold increase in the rate of wound closure following Dm-Kat60 RNAi (Fig. 4b–d). To specify the basis of this difference, we then assessed the intrinsic motility properties of single cells using time-lapse microscopy (Fig. 5a, Movie S2). Dm-Kat60 RNAi-treated cells moved significantly faster than controls with a striking increase in the number of high velocity movements (Fig. 5b,c). They also exhibited an increase in total migration distance (Fig. 5d). Although control D17 cells do not exhibit directional motility in this assay, we did observe a slight, but significant decrease in directionally persistent migration (Fig. 5e), suggesting that the increased wound migration of Dm-Kat60 depleted cells does not result from increased directionality. Finally, we measured a notable difference in persistent migration following Dm-Kat60 RNAi. Whereas migrating control cells spent ~63% of their time moving, cells depleted of Dm-Kat60 spent ~73% of their time migrating (Fig. 5f). Taken together, these data suggest that Dm-Kat60 normally serves as a negative regulator of cell motility by suppressing fast and persistent migration.

Does Katanin regulate the migration of human cells? While conventional human p60 had no apparent impact on cell movement (not shown), the p60-like protein, KATNA1 (KL1)[34,35], does localize to the leading edge of migratory cells, regulate MT growth and negatively impact cell movement (see Supplementary information, Fig. S6a–e). Thus, human KATNA1 is likely the functional orthologue of Dm-Kat60, at least during interphase.

Dm-Kat60 inhibits actin protrusions at the cell edge

MTs are believed to impact cell movement largely through the regulation of actin based structures, such as lamellae[5,36–39]. Unfortunately, technical limitations precluded us from testing these cytoskeletal interactions in D17 cells. However, this could be studied in S2 cells co-expressing GFP- α-tubulin and mCherry-actin. While Dm-Kat60 RNAi did not significantly impact on the accumulation of actin at the cortex or the rate of actin retrograde flow (not whosn), it did strongly influence the cycles of lamellipodium protrusion and retraction. Specifically, Dm-Kat60 RNAi treated cells displayed a significant ~3-fold increase in the frequency of protrusions and >2-fold increase in the average displacement per protrusion (Fig. 6b,c; Movie S3). A localized increase in the protrusion/retraction cycle at the leading edge could conceivably underlie the increased cell migration rates observed following Dm-Kat60 RNAi.

Kat-60 is MT severing enzyme and end depolymerase

Finally, we examined Dm-Kat60's *in vitro* mechanism-of-action using purified, baculovirus-expressed, GFP-Dm-Kat60 (rDm-Kat60). Taxol-stabilized, rhodamine-labeled MTs were immobilized on coverslips[40], incubated with 50 nM rDm-Kat60 (Fig. 7a) and imaged through time using total internal reflection microscopy (TIRF). rDm-Kat60 robustly severed taxol-stabilized MTs in the presence of ATP (Fig. 7b, c; Movie S4) and this reaction was inhibited when ATP was depleted with hexokinase and glucose or replaced with the non-hydrolyzable ATP analogue, AMPPNP (Fig. 7e). Thus, Dm-Kat60-mediated severing is stimulated by ATP hydrolysis. Severing also likely involves an interaction between Dm-Kat60 and the C-terminal tail of tubulin since it was almost completely inhibited by the protease subtilisin, which removes the C-termini of the tubulin subunits within the MT polymer (not shown). Subtilisin treatment was previously reported to inhibit Katanin-mediated severing of MTs[8].

To our surprise, we also observed substantial rDm-Kat60-induced depolymerization of MT ends which generally preceded any obvious severing of the lattice (Fig. 7b, c). Like severing, end-depolymerization was suppressed by hexokinase and glucose, AMPPNP and subtilisin suggesting that both occur by a similar mechanism (Fig. 7e). While both MT ends were depolymerized by rDm-Kat60, one end almost always depolymerized faster than the other (Fig. 7c). When these assays were performed using polarity marked MTs, the plus-end was found to depolymerize ~3-fold faster than the minus-ends (Fig. 7d, e). To ensure that MT end depolymerization did not result from a protein contaminant, identical analyses were performed using the catalytically inactive Dm-Kat60 (E393Q)[41] mutant. This mutant was entirely incapable of severing MTs and, while it did induce some end depolymerization, the rate at which this occurred was ~5-fold slower than that induced by the wild type protein (Fig. 7e).

In a last set of experiments we examined the morphology of MT ends severed/depolymerized by rDm-Kat60 using electron microscopy (EM). Samples of MTs incubated with rDm-Kat60 and ATP, rDm-Kat60 and AMPPNP, and a no rDm-Kat60 control were applied to EM grids and fixed by negative staining (Fig. 7f). We measured a ~3-fold increase in the number of MT ends/unit length in the rDm-Kat60/ATP condition relative to the AMPPNP and no-rDm-Kat60 controls (Fig. 7g). Thus, rDm-Kat60 was active in these assays. Interestingly, we observed no substantial difference in the morphology of MT ends among any of the above conditions. In all cases, MT ends were blunt or had a few straight protofilaments protruding from the end. By contrast, MTs incubated with the *Drosophila* kinesin-13, Klp59D[42], displayed numerous curled protofilaments peeling away from the ends (Fig. 7g) which is typical of kinesin-13 catalysed MT depolymerization[43]. This suggests that that Dm-Kat60 and kinesin-13s remove tubulin from MT ends via distinct mechanisms

Discussion

Our results identify Dm-Kat60 as a novel and important regulator of microtubule dynamics and cell migration. The human Katanin, KATNA1, behaves similarly. In addition to its cellular roles, *in vitro* analyses indicate that Dm-Kat60 has the capacity to function both as a MT severing enzyme and end-depolymerase which, to our knowledge, is an unprecedented observation. Based on its cortical localization, RNAi phenotypes, and catalytic activity, we propose that Dm-Kat60 (and KATNA1) contributes to the generation of a dynamic interface between the MT cytoskeleton and the interphase cortex by removing tubulin subunits from any region of the MT making contact Dm-Kat60-rich cortical sites (see Supplementary information, Fig. S7).

Among the more unexpected outcomes of this study is the observation that Dm-Kat60 induces MT end depolymerization, *in vitro*. However, given current models of Katanin's interaction with the MT, such a finding is not entirely surprising. Biophysical and biochemical studies have suggested that severing by Katanin is mediated by the transient hexamerization of p60 proteins about the C-terminus of a single tubulin within the MT[7,41]. ATP-hydrolysis and/or the subsequent disassembly of the hexamer is believed to generate a mechanical force which, through multiple iterations, induces the removal of the tubulin from the lattice. If Katanin works by "tugging" on a single tubulin heterodimer, then the exposed tubulins at the microtubule end are likely to be the easiest to remove because they lack a longitudinal contact. However, we cannot rule out the possibility that Dm-Kat60-mediated end-depolymerization is a manifestation of multiple severing events occurring very near the tip.

Within the cell, Dm-Kat60's severing and depolymerase activities likely remain under very tight spatial constraints. In this regard, the recruitment of Dm-Kat60 to the cell cortex appears to be central to its interphase functions. While our data suggest that this process is reliant on the presence of actin but not MTs, the specific mechanisms that deliver Dm-Kat60 to the cortex remain a mystery. One appealing hypothesis is that Dm-Kat60 is directly or indirectly linked to the cortical actin array via *Drosophila* p80. The p80 subunit contains repeated WD40 motifs known to mediate protein-protein interactions[44]; similar motifs have been identified in some actin-binding proteins[45]. p80's WD40 repeats are essential for the centrosomal targeting of Katanin in other organisms[46,47]. It has also been suggested that p60 acts independently of p80 in some circumstances[48]. The identification of Dm-Kat60's binding partners represent an important next step in understanding its cellular activities.

At the cortex, Dm-Kat60 suppresses MT growth primarily by inducing plus-end catastrophes and transitions from growth to pause. While other classes of proteins are known to induce MT depolymerization, *in vitro*[43,49–51], Dm-Kat60's presumptive ability to remove tubulins from any region of the MT—end or lattice—may be particularly useful in the more complex cellular environment. For example, such an activity could allow Dm-Kat60 to prevent sustained MT growth along the cortex regardless of whether the MT contacts the cortex end-on or side-on. The newly created plus-end at the cortical MT interface would then initiate catastrophe or enter the pause state depending on its association with other MT binding proteins (see below). Moreover, the ends of polymerizing MTs in cells are often "capped" by plus-end binding proteins such as EB1[52]. Dm-Kat60 could remove these by severing the MT at the base of the EB1 "cap" and/or directly removing EB1-bound tubulins from the plus-end. The acidic tail of EB1 could mimic the C-terminus of tubulin thereby providing a substrate for Dm-Kat60[53].

Of course, Dm-Kat60 is not alone in its ability to stimulate the catastrophe of MT plus-ends near the cortex of interphase S2 cells as the *Drosophila* kinesin-13, KLP10A also displays this activity[24]. However, aside from the ability of both proteins to promote catastrophes, the activities of Dm-Kat60 and KLP10A are quite distinct. A most notable difference is that KLP10A does not concentrate on the cortex but instead binds to the ends of polymerizing MTs to which it is recruited by EB1. Intriguingly, recent work suggests that EB1 can inhibit the depolymerase activity of Kinesin-13s by shielding the plus-end[54]. If Dm-Kat60 were to generate plus-ends lacking EB1, then it could relieve this inhibition. .

We propose that Dm-Kat60 and KLP10A work together as follows: 1) Dm-Kat60 removes tubulins (EB1-bound or otherwise) from regions of the MT that come in close proximity to the cortex thereby creating a free plus-end at the cortical interface. Many of these newly created plus-ends immediately enter a paused state (depletion of EB1 has been shown to strongly promote pause[55]). 2) Next, KLP10A, which has already been accumulated near the

end by EB1, promotes the transition of this end from pause to shrinkage—this transition can occur rapidly and may often appear as a catastrophe. Our current study also suggests that KLP10A increases the rate of plus-end depolymerization and thus a small, difficult to detect, portion of the protein may remain associated with the end as it depolymerizes. Why such an effect was not noted in our initial analysis of KLP10A is unknown but may be due to the more limited region of the cortex analyzed in that study[24].

The finding that Dm-Kat60 targets to the leading edge of motile D17 cells and alters their migration provides a broader biological context through which our findings can be viewed and interpreted. While Dm-Kat60's depletion had no obvious influence on the establishment cell polarity, it did increase both the frequency and displacement of membrane protrusions, at least in S2 cells. The localized suppression of protrusions at the leading edge of motile D17 cells could exert negative control over the rate and persistence of cell movement.

The observation that Dm-Kat60 RNAi results in faster and more persistent migration seems consistent with other studies demonstrating that growing MTs stimulate the GTPase, Rac, at the leading edge, which may promote adhesion complex remodeling needed to drive and sustain protrusions[38,39]. In addition, because Dm-Kat60 depletion at the leading edge of migratory cells should decrease catastrophes, MTs could become unusually persistent and abundant in the extending protrusion, which may intensify other processes that favor protrusion, like increased kinesin-mediated delivery of vesicles to the protrusion zone[56].

How does this relate to the organism? A recent study examining hemocyte migration in developing *Drosophila* embryos, for which we believe D17 cells to be a model, showed that hemocytes migrate less efficiently in response to guidance cues following the disruption of MT dynamics[30]. Under these conditions, the authors also observed an increase in cell velocities and decrease in directional persistence - similar to D17 cells depleted of Dm-Kat60 by RNAi. Thus, Dm-Kat60 at the leading edge may modulate MT dynamics to "fine-tune" cell migration by suppressing protrusions.

In conclusion, the findings of this study uncover new and unexpected roles for the *Drosophila* Katanin p60, Dm-Kat60, in the regulation of cortical MT dynamics and provide insights into how the MT cytoskeleton feeds into cell migration. The ability of cells to move and change shape is central to organismal development and when defective have been linked to human diseases such as cancer. Given this, our finding that human KATNA1 performs many of the same functions as Dm-Kat60 suggest the former as a potentially useful new therapeutic target.

METHODS

S2 cell culture, RNAi and construction of plasmids

S2 cells expressing GFP-α-tubulin were a gift from R. Vale (University of California, San Francisco, CA). Wild-type S2 cells were obtained from ATCC (Manassas, VA). Our methods for S2 cell culture, RNAi treatment of S2 cells, and production of dsRNA from the 3′ UTR of endogenous Dm-Kat60 (including sequences) were described previously[12].

Immunofluorescence microscopy

S2 cells were plated on concanavalin A-coated coverslips for 1.5 hrs, fixed in 100% methanol at −20°C for 20 min and blocked with 5% normal goat serum in PBS containing 0.1% Triton X-100. Primary antibodies (Dm-Kat60, α-tubulin [DM1a; Sigma-Aldrich, St. Louis, MO], and actin [clone C4, Millipore, Billerica, MA]) were applied at 1–20 μg ml^{-1} final concentration in blocking buffer. Fluorescent secondary antibodies (Jackson Immuno-Research Laboratories, West Grove, PA) were used at 7.5 μg ml^{-1}. Imaging was performed

on an Ultraview spinning-disk confocal system (PerkinElmer, Waltham, MA) mounted on an inverted microscope (Eclipse TE300; Nikon) with a 100× (1.4 NA) or 60× (1.4 NA) objective and captured with an Orca ER digital camera (Hamamatsu, Japan). For MT disruption, cells were treated with 50 μM colchicine for 18 hrs prior to fixation. For microfilament disruption, cells were treated with 5 μM cytochalasin D for 1 hr before fixation.

Live cell imaging and automated tracking

4D time-lapse movies of GFP-α-tubulin-expressing S2 cells were acquired using the Ultraview spinning disk confocal microscope described above. MT ends were tracked through each series of time-lapse images with an automated tracking program using the following assumptions:

Definition of the tracking region—For each cell, we tracked MTs in a hand-selected region-of-interest (ROI) consisting of an outer (the cortex; Fig. 3a) and an inner (to avoid tracking into the crowded interior) boundary. For all calculations, the data from cells of the same treatment (control or Dm-Kat60 RNAi) were pooled.

Definition of growth and shrinkage—To define growth and shortening, we calculated the angle α between the direction of the displacement of the MT tip and the direction of the MT itself. A value of $\cos(\alpha)>0.2$ ($\alpha<\sim78°$) indicated probable growth, and $\cos(\alpha)<-0.2$ ($\alpha>\sim101°$) indicated probable shortening. These "loose" cutoffs were chosen to deal with the curvature of MTs in the Dm-Kat60 RNAi cells. To qualify as growing or shortening, we required that the MT display the same behavior (either growing or shortening) for at least two consecutive frames, and that the overall displacement in a run of growth or shrinkage be at least 5 pixels.

Definition of the distance to the cortex—Distance to the cortex was defined as the Euclidean distance from a MT tip to its closest point on the cortex. The difference in the distance distributions was tested using the Kolmogorov-Smirnov two-distribution test.

Definition of growth parallel to the cortex—For two consecutive frames t and $t+1$, the points on the cortex closest to the trajectory segment are given by $\mathbf{c}(t+1)$ and $\mathbf{c}(t)$, respectively, and the displacement vector along the cortex is $\delta\mathbf{c}(t)=\mathbf{c}(t+1)-\mathbf{c}(t)$. A MT was considered to grow parallel to the cortex if the angle between the tip displacement and $\delta\mathbf{c}(t)$ was less than 45°. Error bars plotted are the asymptotic standard errors for a binomial distribution: $\sqrt{p(1-p)/N}$, where p is the fraction that grow along the cortex, and N is the total number of data points. Significance was tested by χ^2 using a 2×2 table of dichotomous outcomes.

Calculating transition rates—Catastrophes near the cortex were determined by counting the number of significant shortening events away from the cortex. To be counted, a shortening event had to begin within 0.63 μm of the cortex (10 pixels), and increase its distance from the cortex by at least 0.32 μm (5 pixels) by the end of the shortening run. The catastrophe statistic was calculated as

$$\frac{1}{N}\sum_{i=1}^{N}\left[\frac{[\text{depolymerization events in cell } i]/[\text{s in cell } i]}{[\text{microtubules near cortex in cell } i]}\right]$$

The standard error was estimated by bootstrap sampling on the terms of the sum with 1000 resamples. Statistical significance was determined using 1000 resamples of a one-sided permutation test with the test statistic $\log(S_{1,i}/S_{2,i})$, where $S_{1,i}$ and $S_{2,i}$ are the catastrophe statistic sums for resample i of control (1) and Dm-Kat60 RNAi (2), respectively. To calculate transition rates (Table 1), each frame of a MT trajectory was marked as either grow, shorten, or pause. Grow and shorten states were defined as previously described. Pause was defined as neither growing nor shortening. The lifetimes of states that began and ended in the middle of a trajectory (not on a boundary), as well as the state they transitioned to, were collected. The rate of transition between an initial state k (k=grow, shrink, or pause) and a final state l (l≠k) is

$$\frac{[\text{no.of transitions from } k \text{ to } l]}{[\text{no.of transitions out of } k]} \times \frac{1}{[\text{no.of transitions out of } k]} \times \sum_i \left(\frac{1}{[\text{time in state } k \text{ before transition } i]} \right)$$

We used a bootstrap approximation to construct 95% confidence intervals of each transition, with 1000 resamples of all lifetimes. Statistical significance was established using a two-sided permutation test with 1000 resamples of the statistic $r_{1,i} - r_{2,i}$, where $r_{1,i}$ and $r_{2,i}$ correspond to the rates calculated in resample i of control (1) and Kat60-RNAi (2).

Purification of recombinant 6xHis-GFP-Dm-Kat60

6xHis-GFP-Dm-Kat60 (rDm-Kat60) was cloned into pFastBac HTa (Invitrogen) and then transformed into DH10Bac E. coli cells. The primers to amplify GFP were: forward—GAATTCACCATGGTGAGCAAGGGCGAGGAG and reverse—AAGGAAAAAAGCGGCCGCCTTGTACAGCTCGTCCATGCCGAG. The primers to amplify Dm-Kat-60 were: forward—AAGGAAAAAAGCGGCCGCCACCATGTCCATAACCTTACTGCGAGGTGG and reverse—CCGCTCGAGTCATGACGATCCGAACTCCCTC.

The bacmid was isolated from DH10Bac E. coli and then transfected into Sf9 cells. The virus-containing supernatant was used to infect fresh Sf9 cells for 72 hrs and procedure was repeated twice to amplify the baculovirus. 20 μl of the third cycle supernatant was added to Sf9 cells in 250 ml SFM900-II medium (Invitrogen) with 5% FBS to express 6xHis-GFP-Dm-Kat60 at a low level (high levels of expression yielded inactive aggregates). Infected cells were lysed with a French press, centrifuged, and the resulting supernatant incubated with 1ml nickel resin (Qiagen) at 4 °C for 1 hr. The resin was then transferred into 20ml chromatography column (Biorad) and washed with 4 column volumes of wash buffer (40 mM imidazole in resuspension buffer without PMSF), and eluted with 500 mM imidazole in resuspension buffer without PMSF. The eluted rDm-Kat60 was concentrated by centrifugation and exchanged into severing buffer I (20 mM HEPES, pH 7.0, 300 mM NaCl, 3 mM $MgCl_2$, 10% sucrose, 50 μM ATP, 5 mM DTT).

In vitro assays

Rhodamine-labeled, taxol-stabilized non-polarity or polarity-marked MTs were prepared according to an online protocol (http://mitchison.med.harvard.edu/protocols.html) and immobilized in the flow chamber with a kinesin rigor mutant (G234A) as reported[40]. The assay was conducted in severing buffer II (20 mM HEPES, pH 7.0, 100 mM NaCl, 3 mM $MgCl_2$, 10% sucrose, 2 mM ATP, 10 mM DTT, 7.5 mg/ml BSA, 0.1% Pluronic F-127) at 24 °C. An oxygen-scavenger system (220 μg/ml glucose oxidase, 22.5 mM glucose, 36 μg/ml catalase) was included to minimize photodamage. In some control assays, 5 mM AMP-PNP or 4 mM hexokinase was used in place of ATP. Subtilisin-pretreatment of MTs was the

same as reported[7]. After perfusing MTs into the flow chamber cell, the purified rDm-Kat60 construct was introduced into the chamber and fluorescent MTs were imaged by Total internal reflection microscopy (TIRF). Our TIRF microscope used a home-made laser system assembled around a Nikon Eclipse Ti microscope and a high numerical aperture objective (60x, NA=1.49).

Digital images were saved as stacks of TIFF files, and time-lapse series were saved as AVI videos. Kymographs were generated using the Multiple Kymograph plug-in (ImageJ). From the kymographs of all MTs recorded for each treatment of the depolymerization assay, we calculated the average angle of the MT ends' displacements through time. The depolymerization rate was determined by calculating the reciprocal of the tangent of the average angle, and then applying the appropriate conversions to derive the distance and time values. The *in vitro* severing frequency was determined by manually counting the number of severing events in every MT. The number of severing events in a single movie was divided by the total length of the MTs at the start of the movie and divided by the total time of the movie.

D17 cell RNAi and migration assays

D17 cells were maintained in a RT incubator in D17 medium: Schneider's medium (Invitrogen) supplemented with 10% FBS (Gibco), 1% antibiotic-antimycotic (Gibco), and 1.25 μg/mL insulin (Invitrogen).

For RNAi, D17 cells were treated on days 0, 2, 4, 6, and 8 with 20 μg of dsRNA in 1 mL serum-containing Schneider cell medium (Life Technologies). On day 9, the RNAi-treated cells were either plated on ECM-coated plastic tissue culture dishes for wound-healing experiments or ECM-coated glass-bottom tissue culture dishes for single-cell analysis. For wound-healing experiments, cells were allowed to adhere for 4–6 hr before manually scraping the cell monolayer with a pipette tip. After replenishing the medium, the scratch-wound regions were imaged 0 hr and 24 hr after wounding using a phase-contrast microscope. For single-cell analysis, cells were imaged every 3 min for 3 hr using a phase-contrast microscope equipped with a 10x (0.25 NA) objective.

Electron microscopy

Samples for negative stain electron microscope experiments were prepared by mixing 1.5 μM of MTs with 50 nM rDm-Kat60 in severing buffer II (above) for 30 min at 24 °C. 5 μl of this mixture was then loaded onto freshly glow-discharged carbon supported grids (Electron Microscopy Sciences, Hatfield, PA). The grid was washed and stained with 1% uranyl acetate, followed by observation in a Tecnai F20 microscope (FEI, Eindhoven, The Netherlands) operating at 120 kV with a nominal magnification of x50,000.

Statistics

Differences between treatments were analyzed using either a one-way nonparametric analysis of variance (Kruskal-Wallis) for multiple group comparisons or a nonparametric t test (Mann-Whitney) for two group comparisons (SigmaStat, Systat Software; or GraphPad Prism, GraphPad Software). Measurement means were taken to be statistically different if $P < 0.05$.

Supplementary Material

Refer to Web version on PubMed Central for supplementary material.

Acknowledgments

DJS, UR and DZ were supported by NIH grant # R01-GM065940 (to DJS). SLR, KDG, and JC and were supported by March of Dimes grant # 1-FY08-429 and NIH grant # R01 GM081645 (both to SLR). SS and AM were supported by NIH grant # R01-GM086536 (to AM). JLR and DD were supported by March of Dimes grant # 5-FY09-47 (to JLR). HJS, AA, EL and TR were supported by NIH grant # R01-GM083338 (to HJS).

References

1. van der Vaart B, Akhmanova A, Straube A. Regulation of microtubule dynamic instability. Biochem Soc Trans. 2009; 37:1007–1013. BST0371007 [pii]. 10.1042/BST0371007 [PubMed: 19754441]
2. Jaworski J, Hoogenraad CC, Akhmanova A. Microtubule plus-end tracking proteins in differentiated mammalian cells. Int J Biochem Cell Biol. 2008; 40:619–637. S1357-2725(07)00336-6 [pii]. 10.1016/j.biocel.2007.10.015 [PubMed: 18023603]
3. Martin SG. Microtubule-dependent cell morphogenesis in the fission yeast. Trends Cell Biol. 2009; 19:447–454. S0962-8924(09)00140-8 [pii]. 10.1016/j.tcb.2009.06.003 [PubMed: 19713114]
4. Siegrist SE, Doe CQ. Microtubule-induced cortical cell polarity. Genes Dev. 2007; 21:483–496. 21/5/483 [pii]. 10.1101/gad.1511207 [PubMed: 17344411]
5. Watanabe T, Noritake J, Kaibuchi K. Regulation of microtubules in cell migration. Trends Cell Biol. 2005; 15:76–83. S0962-8924(04)00338-1 [pii]. 10.1016/j.tcb.2004.12.006 [PubMed: 15695094]
6. Siller KH, Doe CQ. Spindle orientation during asymmetric cell division. Nat Cell Biol. 2009; 11:365–374. ncb0409-365 [pii]. 10.1038/ncb0409-365 [PubMed: 19337318]
7. Roll-Mecak A, McNally FJ. Microtubule-severing enzymes. Curr Opin Cell Biol. 2010; 22:96–103. S0955-0674(09)00194-X [pii]. 10.1016/j.ceb.2009.11.001 [PubMed: 19963362]
8. McNally FJ, Vale RD. Identification of katanin, an ATPase that severs and disassembles stable microtubules. Cell. 1993; 75:419–429. 0092-8674(93)90377-3 [pii]. [PubMed: 8221885]
9. Buster D, McNally K, McNally FJ. Katanin inhibition prevents the redistribution of gamma-tubulin at mitosis. J Cell Sci. 2002; 115:1083–1092. [PubMed: 11870226]
10. McNally K, Audhya A, Oegema K, McNally FJ. Katanin controls mitotic and meiotic spindle length. J Cell Biol. 2006; 175:881–891. jcb.200608117 [pii]. 10.1083/jcb.200608117 [PubMed: 17178907]
11. Srayko M, O'Toole ET, Hyman AA, Muller-Reichert T. Katanin disrupts the microtubule lattice and increases polymer number in C. elegans meiosis. Curr Biol. 2006; 16:1944–1949. S0960-9822(06)02041-0 [pii]. 10.1016/j.cub.2006.08.029 [PubMed: 17027492]
12. Zhang D, Rogers GC, Buster DW, Sharp DJ. Three microtubule severing enzymes contribute to the "Pacman-flux" machinery that moves chromosomes. J Cell Biol. 2007; 177:231–242. jcb.200612011 [pii]. 10.1083/jcb.200612011 [PubMed: 17452528]
13. Karabay A, Yu W, Solowska JM, Baird DH, Baas PW. Axonal growth is sensitive to the levels of katanin, a protein that severs microtubules. J Neurosci. 2004; 24:5778–5788. 24/25/5778 [pii]. 10.1523/JNEUROSCI.1382-04.2004 [PubMed: 15215300]
14. Yu W, et al. The microtubule-severing proteins spastin and katanin participate differently in the formation of axonal branches. Mol Biol Cell. 2008; 19:1485–1498. E07-09-0878 [pii]. 10.1091/mbc.E07-09-0878 [PubMed: 18234839]
15. Casanova M, et al. Microtubule-severing proteins are involved in flagellar length control and mitosis in Trypanosomatids. Mol Microbiol. 2009; 71:1353–1370. MMI6594 [pii]. 10.1111/j.1365-2958.2009.06594.x [PubMed: 19183280]
16. Quarmby L. Cellular Samurai: katanin and the severing of microtubules. J Cell Sci. 2000; 113(Pt 16):2821–2827. [PubMed: 10910766]
17. Rasi MQ, Parker JD, Feldman JL, Marshall WF, Quarmby LM. Katanin knockdown supports a role for microtubule severing in release of basal bodies before mitosis in Chlamydomonas. Mol Biol Cell. 2009; 20:379–388. E07-10-1007 [pii]. 10.1091/mbc.E07-10-1007 [PubMed: 19005222]
18. Sharma N, et al. Katanin regulates dynamics of microtubules and biogenesis of motile cilia. J Cell Biol. 2007; 178:1065–1079. jcb.200704021 [pii]. 10.1083/jcb.200704021 [PubMed: 17846175]

19. Stoppin-Mellet V, et al. Arabidopsis katanin binds microtubules using a multimeric microtubule-binding domain. Plant Physiol Biochem. 2007; 45:867–877. S0981-9428(07)00182-9 [pii]. 10.1016/j.plaphy.2007.09.005 [PubMed: 17977001]
20. Stoppin-Mellet V, Gaillard J, Vantard M. Katanin's severing activity favors bundling of cortical microtubules in plants. Plant J. 2006; 46:1009–1017. TPJ2761 [pii]. 10.1111/j.1365-313X.2006.02761.x [PubMed: 16805733]
21. Burk DH, Zhong RQ, Ye ZH. The katanin microtubule severing protein in plants. J Integr Plant Biol. 2007; 49:1174–1182.10.1111/j.1672-9072.2007.00544.x
22. Burk DH, Liu B, Zhong RQ, Morrison WH, Ye ZH. A katanin-like protein regulates normal cell wall biosynthesis and cell elongation. Plant Cell. 2001; 13:807–827. [PubMed: 11283338]
23. Nakamura M, Ehrhardt DW, Hashimoto T. Microtubule and katanin-dependent dynamics of microtubule nucleation complexes in the acentrosomal Arabidopsis cortical array. Nat Cell Biol. 2010; 12:1064–1070. ncb2110 [pii]. 10.1038/ncb2110 [PubMed: 20935636]
24. Mennella V, et al. Functionally distinct kinesin-13 family members cooperate to regulate microtubule dynamics during interphase. Nature Cell Biology. 2005; 7:235–U239.10.1038/Ncb1222
25. Ozon S, Guichet A, Gavet O, Roth S, Sobel A. Drosophila stathmin: a microtubule-destabilizing factor involved in nervous system formation. Mol Biol Cell. 2002; 13:698–710.10.1091/mbc.01-07-0362 [PubMed: 11854423]
26. Lee H, et al. The microtubule plus end tracking protein Orbit/MAST/CLASP acts downstream of the tyrosine kinase Abl in mediating axon guidance. Neuron. 2004; 42:913–926. S0896627304003046 [pii]. 10.1016/j.neuron.2004.05. 020 [PubMed: 15207236]
27. Jankovics F, Brunner D. Transiently reorganized microtubules are essential for zippering during dorsal closure in Drosophila melanogaster. Dev Cell. 2006; 11:375–385. S1534-5807(06)00315-7 [pii]. 10.1016/j.devcel.2006.07.014 [PubMed: 16908221]
28. Borghese L, et al. Systematic analysis of the transcriptional switch inducing migration of border cells. Dev Cell. 2006; 10:497–508. S1534-5807(06)00065-7 [pii]. 10.1016/j.devcel.2006.02.004 [PubMed: 16580994]
29. Ui K, Ueda R, Miyake T. Cell lines from imaginal discs of Drosophila melanogaster. In Vitro Cell Dev Biol. 1987; 23:707–711. [PubMed: 3117765]
30. Stramer B, et al. Clasp-mediated microtubule bundling regulates persistent motility and contact repulsion in Drosophila macrophages in vivo. J Cell Biol. 2010; 189:681–689. jcb.200912134 [pii]. 10.1083/jcb.200912134 [PubMed: 20457764]
31. Kurtti TJ, Brooks MA. Growth and differentiation of lepidopteran myoblasts in vitro. Exp Cell Res. 1970; 61:407–412. [PubMed: 5459839]
32. Merchant D, Ertl RL, Rennard SI, Stanley DW, Miller JS. Eicosanoids mediate insect hemocyte migration. J Insect Physiol. 2008; 54:215–221. S0022-1910(07)00211-9 [pii]. 10.1016/j.jinsphys.2007.09.004 [PubMed: 17996890]
33. Roll-Mecak A, Vale RD. The Drosophila homologue of the hereditary spastic paraplegia protein, spastin, severs and disassembles microtubules. Curr Biol. 2005; 15:650–655. S0960-9822(05)00170-3 [pii]. 10.1016/j.cub.2005.02.029 [PubMed: 15823537]
34. Torres JZ, Miller JJ, Jackson PK. High-throughput generation of tagged stable cell lines for proteomic analysis. Proteomics. 2009; 9:2888–2891.10.1002/pmic.200800873 [PubMed: 19405035]
35. Sonbuchner TM, Rath U, Sharp DJ. KL1 is a novel microtubule severing enzyme that regulates mitotic spindle architecture. Cell Cycle. 2010; 9 11916 [pii].
36. Waterman-Storer C, et al. Microtubules remodel actomyosin networks in Xenopus egg extracts via two mechanisms of F-actin transport. J Cell Biol. 2000; 150:361–376. [PubMed: 10908578]
37. Watanabe T, Noritake J, Kaibuchi K. Roles of IQGAP1 in cell polarization and migration. Novartis Found Symp. 2005; 269:92–101. discussion 101-105, 223-130. [PubMed: 16355537]
38. Waterman-Storer CM, Salmon ED. Actomyosin-based retrograde flow of microtubules in the lamella of migrating epithelial cells influences microtubule dynamic instability and turnover and is associated with microtubule breakage and treadmilling. J Cell Biol. 1997; 139:417–434. [PubMed: 9334345]

39. Waterman-Storer CM, Worthylake RA, Liu BP, Burridge K, Salmon ED. Microtubule growth activates Rac1 to promote lamellipodial protrusion in fibroblasts. Nat Cell Biol. 1999; 1:45–50.10.1038/9018 [PubMed: 10559863]
40. McNally FJ, Thomas S. Katanin is responsible for the M-phase microtubule-severing activity in Xenopus eggs. Mol Biol Cell. 1998; 9:1847–1861. [PubMed: 9658175]
41. Hartman JJ, Vale RD. Microtubule disassembly by ATP-dependent oligomerization of the AAA enzyme katanin. Science. 1999; 286:782–785. 7918 [pii]. [PubMed: 10531065]
42. Rath U, et al. The Drosophila kinesin-13, KLP59D, impacts Pacman- and Flux-based chromosome movement. Mol Biol Cell. 2009; 20:4696–4705. E09-07-0557 [pii]. 10.1091/mbc.E09-07-0557 [PubMed: 19793918]
43. Desai A, Verma S, Mitchison TJ, Walczak CE. Kin I kinesins are microtubule-destabilizing enzymes. Cell. 1999; 96:69–78. S0092-8674(00)80960-5 [pii]. [PubMed: 9989498]
44. Smith TF, Gaitatzes C, Saxena K, Neer EJ. The WD repeat: a common architecture for diverse functions. Trends Biochem Sci. 1999; 24:181–185. S0968-0004(99)01384-5 [pii]. [PubMed: 10322433]
45. Hudson AM, Cooley L. Understanding the function of actin-binding proteins through genetic analysis of Drosophila oogenesis. Annu Rev Genet. 2002; 36:455–488. [pii]. 10.1146/annurev.genet.36.052802.114101 052802.114101 [PubMed: 12429700]
46. Hartman JJ, et al. Katanin, a microtubule-severing protein, is a novel AAA ATPase that targets to the centrosome using a WD40-containing subunit. Cell. 1998; 93:277–287. S0092-8674(00)81578-0 [pii]. [PubMed: 9568719]
47. McNally KP, Bazirgan OA, McNally FJ. Two domains of p80 katanin regulate microtubule severing and spindle pole targeting by p60 katanin. J Cell Sci. 2000; 113(Pt 9):1623–1633. [PubMed: 10751153]
48. Yu W, et al. Regulation of microtubule severing by katanin subunits during neuronal development. J Neurosci. 2005; 25:5573–5583. 25/23/5573 [pii]. 10.1523/JNEUROSCI.0834-05.2005 [PubMed: 15944385]
49. Varga V, et al. Yeast kinesin-8 depolymerizes microtubules in a length-dependent manner. Nat Cell Biol. 2006; 8:957–962. ncb1462 [pii]. 10.1038/ncb1462 [PubMed: 16906145]
50. Gupta ML Jr, Carvalho P, Roof DM, Pellman D. Plus end-specific depolymerase activity of Kip3, a kinesin-8 protein, explains its role in positioning the yeast mitotic spindle. Nat Cell Biol. 2006; 8:913–923. ncb1457 [pii]. 10.1038/ncb1457 [PubMed: 16906148]
51. Sproul LR, Anderson DJ, Mackey AT, Saunders WS, Gilbert SP. Cik1 targets the minus-end kinesin depolymerase kar3 to microtubule plus ends. Curr Biol. 2005; 15:1420–1427. S0960-9822(05)00760-8 [pii]. 10.1016/j.cub.2005.06.066 [PubMed: 16085496]
52. Mimori-Kiyosue Y, Shiina N, Tsukita S. The dynamic behavior of the APC-binding protein EB1 on the distal ends of microtubules. Curr Biol. 2000; 10:865–868. S0960-9822(00)00600-X [pii]. [PubMed: 10899006]
53. Mishima M, et al. Structural basis for tubulin recognition by cytoplasmic linker protein 170 and its autoinhibition. Proc Natl Acad Sci U S A. 2007; 104:10346–10351. 0703876104 [pii]. 10.1073/pnas.0703876104 [PubMed: 17563362]
54. Montenegro, Gouveia S., et al. In Vitro Reconstitution of the Functional Interplay between MCAK and EB3 at Microtubule Plus Ends. Curr Biol. 2010 S0960-9822(10)01010-9 [pii]. 10.1016/j.cub.2010.08.020
55. Rogers SL, Rogers GC, Sharp DJ, Vale RD. Drosophila EB1 is important for proper assembly, dynamics, and positioning of the mitotic spindle. J Cell Biol. 2002; 158:873–884. jcb.200202032 [pii]. 10.1083/jcb.200202032 [PubMed: 12213835]
56. Reed NA, et al. Microtubule acetylation promotes kinesin-1 binding and transport. Curr Biol. 2006; 16:2166–2172. S0960-9822(06)02207-X [pii]. 10.1016/j.cub.2006.09.014 [PubMed: 17084703]

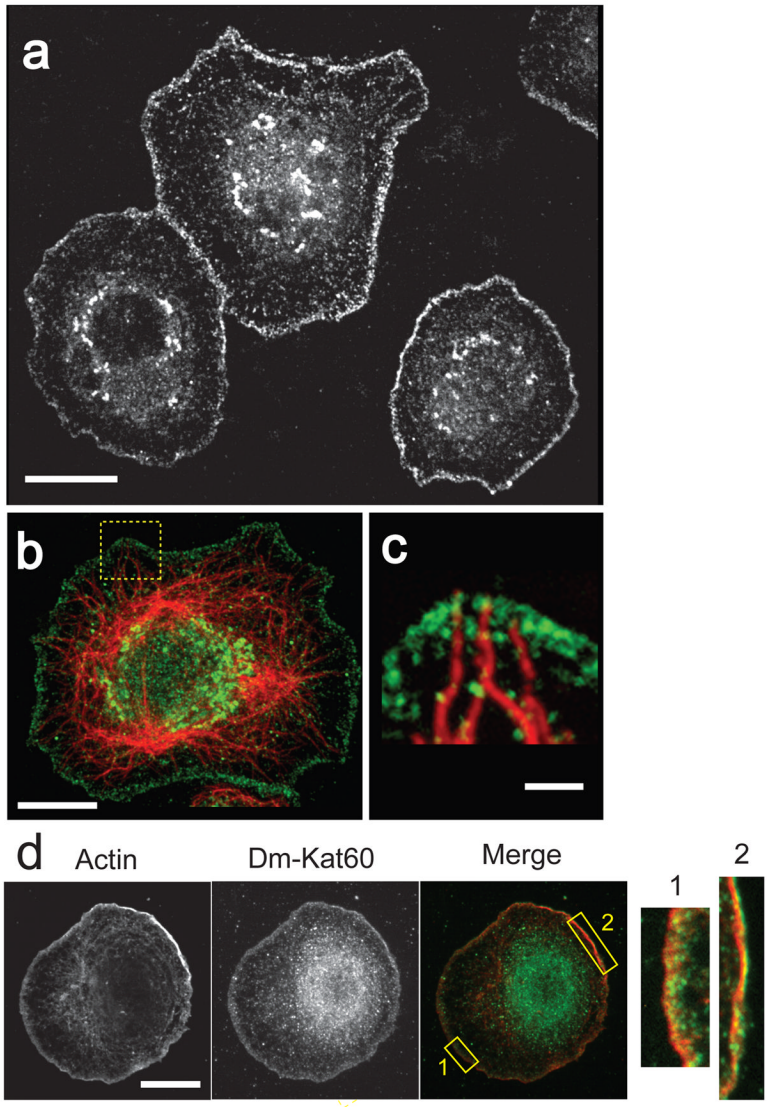

Figure 1. Dm-Kat60 targets to the interphase cell cortex

(a) Immunofluorescence micrograph showing the localization of Dm-Kat60 in interphase S2 cells (antibody characterized in[12]). (b) Immunofluorescence micrograph of an interphase S2 cell double-labeled for MTs (anti-α-tubulin; red) and Dm-Kat60 (green). (c) High magnification of the region boxed in b. (d) Immunofluorescence of an interphase S2 cell double labeled for actin (red) and Dm-Kat60 (green). Higher magnification of the two regions boxed in the “merge” panel. Scale bar, 10 μm (panels a,b,d) or 2 μm (panel c).

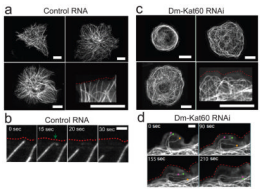

Figure 2. Depletion of Dm-Kat60 causes significant MT curling and bundling beneath the cortex

(a) Confocal images of live GFP-tubulin expressing S2 cells treated with control RNA. The cell border is marked with a dashed red line in the higher magnification image shown in the bottom right. The bottom right panel is also shown in Supplemental movie s1a. (b) Time series of a putative MT severing event at the cortex. The green arrow marks the site of MT breakage and the dashed red line marks the cell border. See also, Supplemental movie S1c. (c) Images of live GFP-tubulin expressing S2 cells treated with Dm-Kat60 RNAi. As in (a), the cell border is marked with a dashed red line in the higher magnification image shown in the bottom right of this panel. This panel is also shown in Supplemental movie S1b. (d) Time series of images obtained from a Dm-Kat60 RNAi treated cell showing the lateral growth of MT ends along the cortex and their subsequent incorporation into the underlying MT array. Individual ends are indicated by colored circles and time (seconds) is labeled in each image. Scale bar, 10 μm (panels a, c), 1 μm (panel b) or 2 μm (panel d).

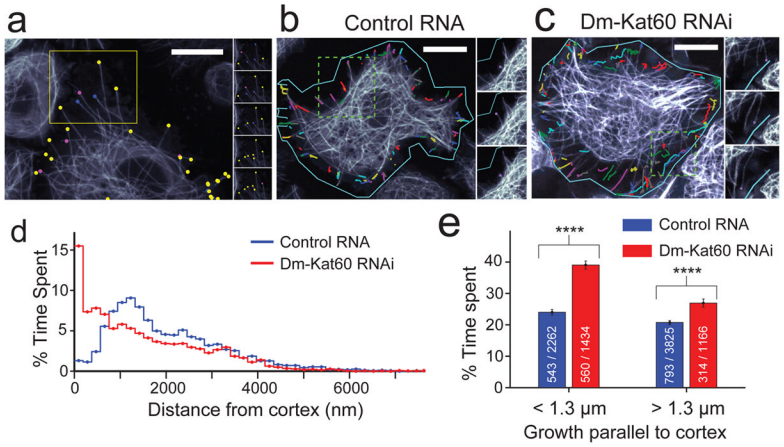

Figure 3. Automated tracking and quantitative analysis of MT plus-end organization and dynamics in control and Dm-Kat60 RNAi treated cells

(a) Ends of GFP-labeled MTs were tracked with an automated tracking algorigthm. Each tracked MT end is marked with a colored dot: growing ends in blue, pausing end in yellow, and shrinking ends in pink. The stack of panels on the right is a time series of the boxed region.

(b) Trajectories of MT ends tracked in a control RNA-treated cells cell. Individual MT trajectory paths are indicated by colored lines. (c) Trajectories of MT ends tracked in a Dm-Kat60 RNAi cell. Again, individual trajectory paths are indicated by colored lines. Relative to controls, significantly more MTs continue to grow after reaching the cortex, and so MTs are frequently observed to bend and grow parallel to the cortex. (d) Compared to control cells (7 cells, 257 MT, 2600 distances), the MT ends in Dm-Kat60 RNAi cells (5 cells, 494 MTs, 6087 distances) spent significantly ($p < 0.0001$) more time in the vicinity of the cortex. MT ends within the cell interior could not be identified and thus were not analyzed. (e) Cortical MTs spend more time growing after Dm-Kat60 knockdown. The change in dynamic behavior is most prominent in MT ends very near (< 1.3 µm) the cell margin, but is still significant ($p < 0.0001$) for ends further (> 1.3 µm) away. Numbers within bars indicate N for cells, and N for MT ends. Error bars, SEM. Scale bars, 10 µm (all image panels).

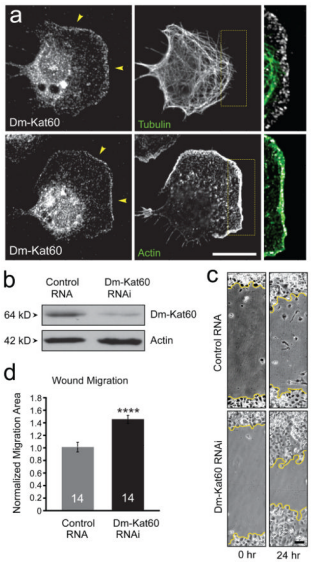

Figure 4. Dm-Kat60 targets to the leading edge of motile D17 cells and negatively regulates their migration

(a) Immunolocalization of Dm-Kat60, tubulin, and actin in polarized *Drosophila* D17 cells. The arrowheads indicate enrichment of Dm-Kat60 at the leading edge; the boxed areas are magnified in far right panels. (b) Western blot showing the depletion of Dm-Kat60 in D17 cells using RNAi (see also Supplemental information, Fig. S8b). (c) Representative phase-contrast images of scratch-wounds at 0 hr and 24 hr after wounding.. (d) Quantification of migration during wound closure for control and Dm-Kat60 RNAi-treated D17 cells. Migration area was calculated by subtracting the total wound area at 24 hr from the total wound area at 0 hr after wounding and then normalized to control RNA. $p = 8.5 \times 10^{-5}$. Data represent mean values ± SEM from four independent experiments. Numbers in bars are sample sizes. Scale bars, 10 μm (panel a) or 50 μm (panel c).

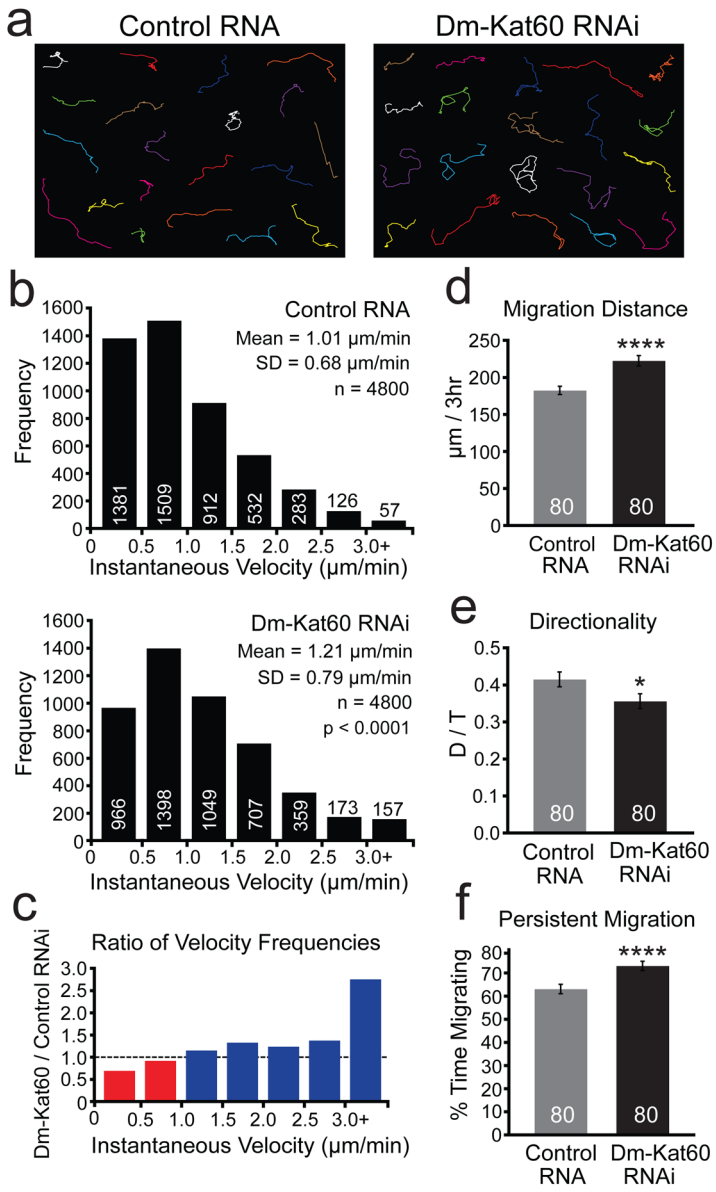

Figure 5. Dm-Kat60 negatively regulates multiple parameters of D17 cell motility

(a) Representative migration tracks of 20 cells for each treatment group (control and Dm-Kat60 RNAi; also see movie S2). (b) Frequency distributions of instantaneous cell velocities from time-lapse imaging of individual D17 cell movements. $p = 8.2 \times 10^{-40}$.

(c) Quantification of the ratio of velocity frequencies between Dm-Kat60 and control RNAi treatments. The Dm-Kat60/control RNAi ratio was calculated by dividing the number of movements for Dm-Kat60 RNAi-treated cells by the number of movements for control RNA-treated cells for a given range of velocities from the graphs in b. A ratio less than one (red) represents a decreased number of movements for Dm-Kat60 RNAi relative to control RNA, and a ratio greater than one (blue) represents an increased number of movements for Dm-Kat60 RNAi relative to control RNA. Relative to control, Dm-Kat60 depletion decreases the frequency of cells migrating at slow rates while increasing the frequency of fast migration rates.

(d) Quantification of total migration distance over a 3 hr time period. $p = 1.5 \times 10^{-5}$. (e) Quantification of intrinsic cell directionality. Directionally persistent migration (D/T) was calculated as a ratio of direct distance between start and end points (D) to the total migration distance (T). $p = 3.6 \times 10^{-2}$.
(f) Quantification of persistent migration. The percentage of time cells spent migrating was calculated by subtracting those movements between frames that were less than 2 μm (considered to be migratory pauses) from the total number of movements and then dividing by the total number of movements. $p = 3.7 \times 10^{-5}$ Data represent mean values ± SEM from four separate dsRNA treatments. Numbers in bars are sample sizes.

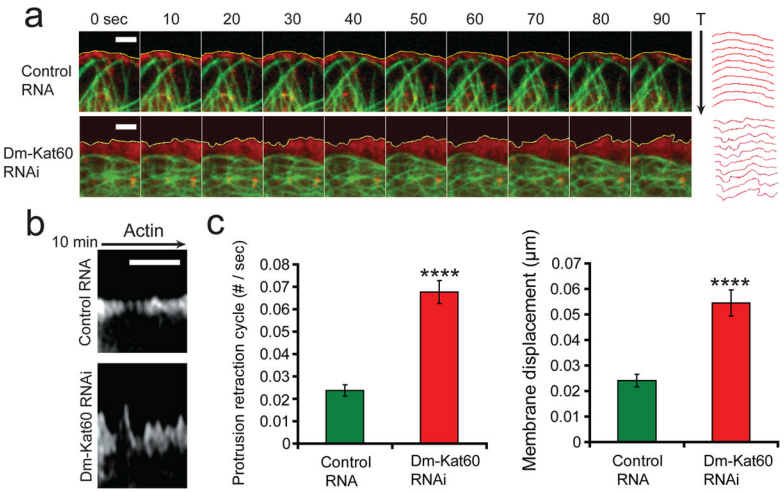

Figure 6. Dm-Kat60 negatively regulates actin protrusions at the cell edge

(a) Time lapse images showing the cortical dynamics of control and Dm-Kat60 RNAi-treated S2 cells expressing GFP-α-tubulin and mcherry-actin. Yellow lines outline the edges of the cortical actin arrays in each image. These lines are stacked vertically (and shown in red) at the far right to illustrate the time-dependent alterations in the morphology of the cell edge (protrusions) in each condition (T shows time axis). (b) Representative kymographs of mcherry-actin labeled cortical regions from a control and Dm-Kat60 RNAi-treated cell. (c). Dm-Kat60 RNAi significantly increases both the frequency (left) and average displacement (right) of actin-based membrane protrusions ($p<0.0001$ for both). Data represent Mean ± SEM and numbers in the columns indicate regions/cells analysed. Scale bars, 2 μm for both panel a and b.

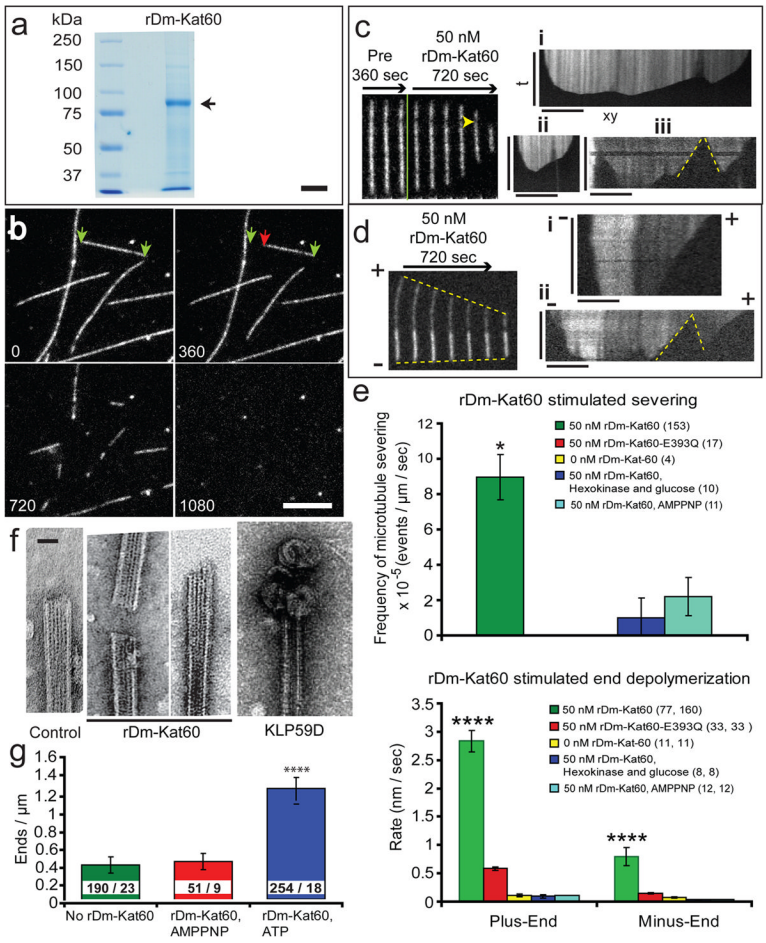

Figure 7. Dm-Kat60 severs and depolymerizes MTs from their ends

(a) Coomassie-stained SDS-PAGE gel of the purified rDm-Kat60 protein used for analysis (see also Supplemental information, Fig. s8c). Arrow indicates the band corresponding to rKat60.

(b) Time-series of TIRF images showing the disassembly of a field of immobilized MTs by 50 nM rDm-Kat60 and ATP. Green arrows mark the ends of an individual MT at the beginning of visualization; a red arrow marks a MT end that has shortened from its initial position. Time (seconds) is indicated.

(c) (Left) Time-series of an individual MT (marked by arrows in c) before (pre) and after addition of rDm-Kat60. i–iii kymographs showing the depolymerization and severing (indicated by dotted yellow lines) of individual MTs from other experiments. The time (t) axis is vertical and distance (xy) axis horizontal in all kymographs shown in this figure

(d) (Left) Time-series of an individual polarity marked MT incubated with rDm-Kat60. The plus-end is dimly labeled and the minus-end is brightly labeled. i & ii. Kymographs showing the depolymerization and severing (dotted yellow lines) of additional polarity marked MTs.

(e) *Upper:* Quantification of the frequency of MT severing by rDm-Kat60. All conditions included 2 mM ATP (or 2 mM AMPPNP). P = 0.031

Lower: Measured rates of MT plus- and minus-end depolymerization by rDm-Kat60. $p = 3.1 \times 10^{-7}$. Again, all conditions included 2 mM ATP or AMPPNP. Data in both panels represent mean ± SEM. N= # of MTs analyzed.

(f) Electon micrographs showing the ends of negatively stained MTs after incubation with: no Dm-Kat60 (control), 50 nM rDm-Kat60 and 2mM ATP (Dm-Kat60), or full-length KLP59D and ATP (KLP59D).

(g). Quantification of MT ends per unit MT length. Compared with the no Dm-Kat60 and Dm-Kat60 (50 nM) + AMPPNP (2mM) controls, Dm-Kat60 + ATP (50 nM GFP-Dm-Kat60, 2 mM ATP) induces 3-fold more ends ($p < 0.0001$). Numbers in the column indicate numbers of MTs/EM fields. Data represent mean ± SEM pooled from two independent experiments.

Scale bars, 500 μm (panel a), 10 μm (panel b) or 20 nm (panel f).

Table 1

Comparison of state-to-state frequency (#/sec) and growth/shrinkage rate (nm/sec) between control, Dm-Kat60RNAi and Klp10A RNAi cells

State-to-state	Control RNA	Dm-Kat60 RNAi	Klp10A RNAi
G → S	0.0106 (34) [a]	0.0041 (7)	0.0028 (4)
	0.0072–0.0144 [b]	0.0017–0.0081	0.0007–0.0073
		p=0.0249 *[c]	p=0.0004 ***
G → P	0.0479(167)	0.0576 (75)*	0.0958 (116)
	0.0432–0.0522	0.0501–0.0645	0.0809–0.1053
		p=0.0225 *	p=0.0181 *
S → G	0.0098 (21)	0.0110 (10)	0.0045 (2)
	0.0063–0.0146	0.0056–0.0195	N/A
		p=0.7687	N/A
S → P	0.0521 (109)	0.0590 (42)	0.1113 (47)
	0.0466–0.0575	0.0477–0.0678	0.0972–0.1242
		p=0.2084	p=0.0035 **
P → G	0.0291 (72)	0.0481 (47)	0.0641 (60)
	0.0223–0.0369	0.0360–0.0627	0.0461–0.0817
		p=0.0145 *	p=0.1778
P → S	0.0216 (77)	0.0156 (22)	0.0119 (14)
	0.0166–0.0275	0.0080–0.0263	0.0059–0.0237
		p=0.2657	p=0.0031 **
Growth	52.79 (1083)	62.13 (580)	58.68 (530)
	1.25 [d]	1.97	1.73
		p<0.0001 ****	p=0.033 *
Shrinkage	84.88 (819)	81.96 (316)	58.43 (179)
	2.81	4.61	3.63
		p=0.8380	p=0.0001 ***

[a] Numbers in parentheses indicate the event count in control RNA (5 cells), Dm-Kat60 RNAi (7 cells) or Klp10A RNAi (5 cells) treatment.

[b] Intervals indicated are 95% confidence intervals calculated using bootstrapping procedure with 1000 resamples, and BCa correction.

[c] * indicates statistically different from control if $p < 0.05$ (p values were shown).

** if $p < 0.01$,

*** if $p < 0.001$, and

**** if $p < 0.0001$. Statistical significance determined using a simulated two-tail permutation test with 1000 resample.

[d] SEM.